Supporting Information

Transforming C_{60} Molecules into Polyhedral Carbon Micro-Nano-Shells for Electrochemically Producing H_2O_2 in Neutral Electrolyte

Rongtao Hu,[a,b] Yaqi Cui,[a] Bing Huang,[a,b] and Lunhui Guan[a]*

a. CAS Key Laboratory of Design and Assembly of Functional Nanostructures, and Fujian Key Laboratory of Nanomaterials, Fujian Institute of Research on the Structure of Matter, Chinese Academy of Sciences, Fuzhou, Fujian 350002, China

b. University of Chinese Academy of Sciences, Beijing 100049, China

Corresponding Author

*Lunhui Guan

E-mail: guanlh@fjirsm.ac.cn

Experimental methods

1. Selection of calcination temperature: Considering the thermogravimetric analysis and the reference [*Angew. Chem. Int. Ed.* **2019**, 58, 3859–3864], we decided the calcination temperature. As shown in **Figure S1**, the thermogravimetric curve displays two prominent mass decrease processes. The first mass decrease process starts at around 200 ºC and ends at around 700 ºC. And the second mass decrease process happens during 700~900 ºC. This means 700 ºC is a critical temperature. Therefore, the sample was heated at 700 ºC and 900 ºC, respectively.

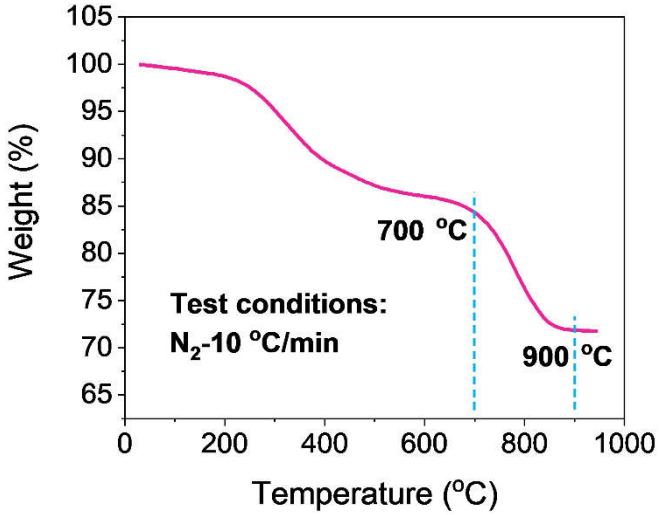

Figure S1. Thermogravimetric curve of "With thiophene". ("With thiophene" is the brown sample obtained after vacuum-filtration and before solid calcination)

2. Calibration of the saturated AgCl/Ag reference electrode:

The calibration of the saturated AgCl/Ag reference electrode was carried out in H_2-saturated 0.1 M KOH solution. The testing system consists of two polished Pt wires (as working electrode and counter electrode, respectively) and the saturated AgCl/Ag reference electrode (as reference electrode). Linear sweep voltametric curve was recorded with scan rate of 1 mV/s. The potential at which the current crosses zero is taken to be the thermodynamic potential (vs. AgCl/Ag) for the hydrogen oxidation reaction (HOR) and hydrogen evolution reaction (HER). As shown in **Figure S2**, the potential is -0.960 V when the current is zero. Therefore, E (vs. RHE) = E (vs. AgCl/Ag) + 0.960 V. (The standard conversion relation is E (vs. RHE) = E (vs. AgCl/Ag) + 0.964 V, 0.964=0.197+0.059×13)

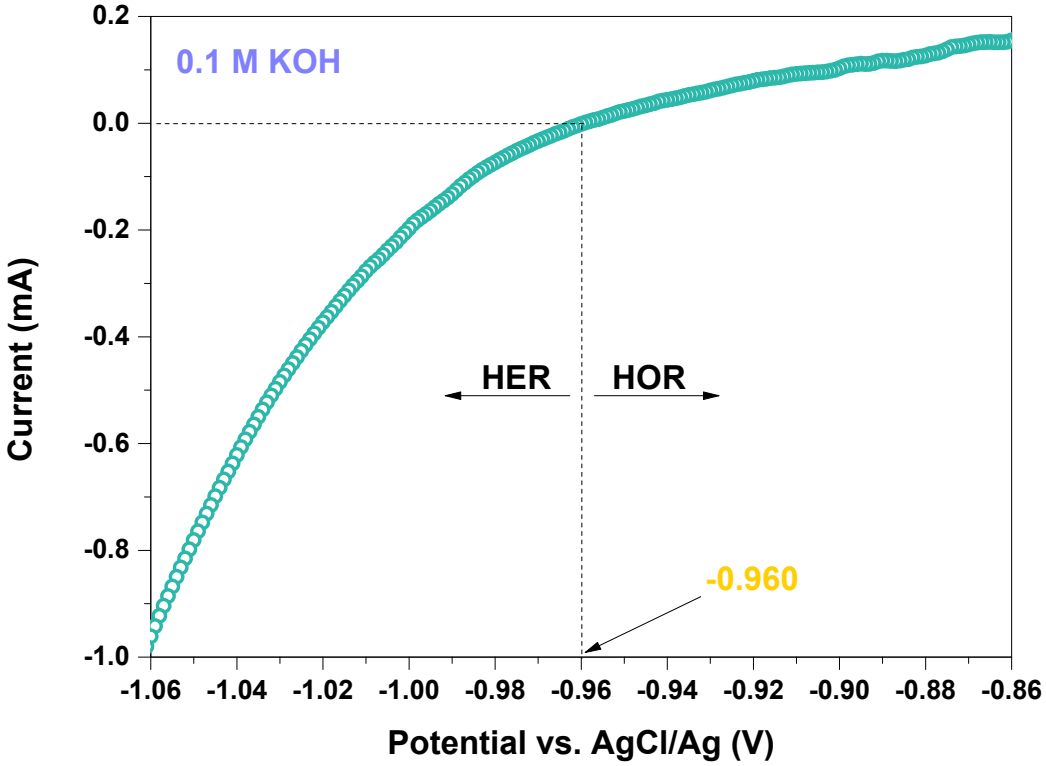

Figure S2. Calibration curve of the saturated AgCl/Ag reference electrode.

3. Calibration of collection efficiency (*N*c) of the Rotating Ring Disk Electrode:

Step 1. Cyclic voltammetry curve was recorded in N_2-saturated 0.1 M KOH- 0.004 M $K_3Fe(CN)_6$/$K_4Fe(CN)_6$ solution with scan rate of 10 mV/s.

Step 2. Amperometric *i-t* curve was recorded 60 s at 1600 rpm in N_2-saturated 0.1 M KOH- 0.004 M $K_3Fe(CN)_6$ solution when the disk electrode was controlled at a constant potential of 0 V (vs. AgCl/Ag, the same later) and the ring electrode was maintained at a constant potential of 0.5 V. As shown in **Figure S3**, the ring current is averaged as 0.260 mA at the last 10 s and the mean disk current of the last 10 s is 0.700 mA. As a result, the collection efficiency of Rotating Ring Disk Electrode is calculated as 0.37.

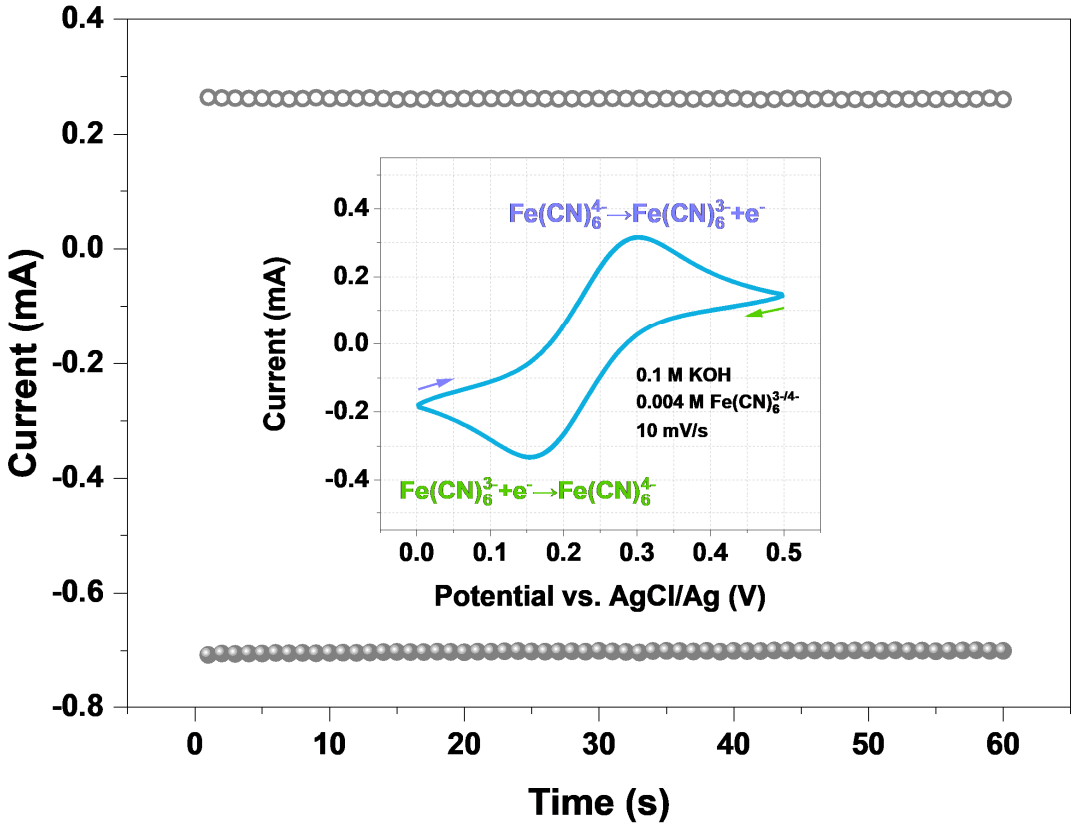

Figure S3. Calibration of collection efficiency (*N*c) of the Rotating Ring Disk Electrode.

4. H-type electrolytic cell test. 20 μL ink was fully coated onto the Carbon paper of 1 cm^2 as the composite electrode (PCMNS/Carbon paper). Two electrolytic tanks separated by activated proton exchange membrane (PEM) were respectively filled with 25.0 mL 0.1 M K_2SO_4. After electrolysis for one specific time interval, 1.0 mL electrolyte was extracted out of the electrolytic tank with working electrode and mixed with 1.0 mL coloring solution (5.0 mM Ce^{4+}). Then, 1.0 mL 0.1 M K_2SO_4 was injected back into that electrolytic tank and the next electrolysis was continued. These steps were repeated until the mixture solution did not appear yellow. These mixture solutions obtained at different electrolytic time were diluted by 10.0 mL 0.1 M K_2SO_4 and transfer 3.0 mL liquid in cuvette for latter Ultraviolet-visible-near infrared absorption spectroscopy.

Results and discussion

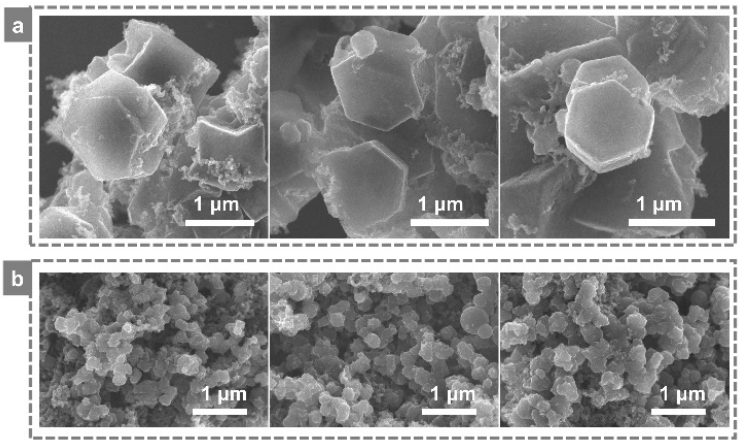

Figure S4. SEM comparison between the polyhedral carbon micro-nano shells (a) and the amorphous carbon nano-aggregates (b).

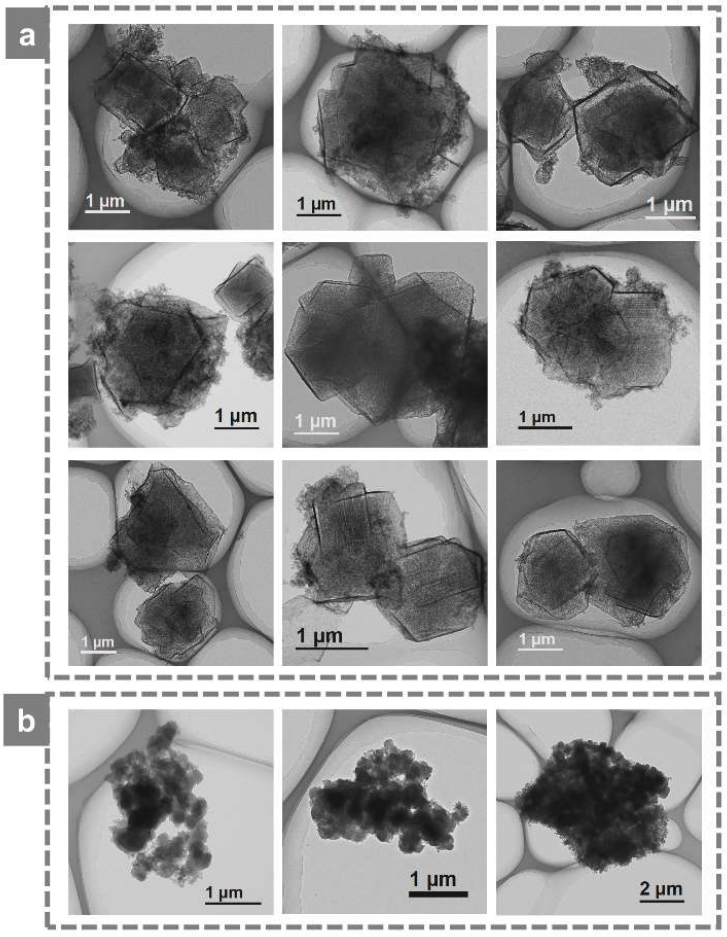

Figure S5. TEM comparison between the polyhedral carbon micro-nano shells (a) and the amorphous carbon nano-aggregates (b).

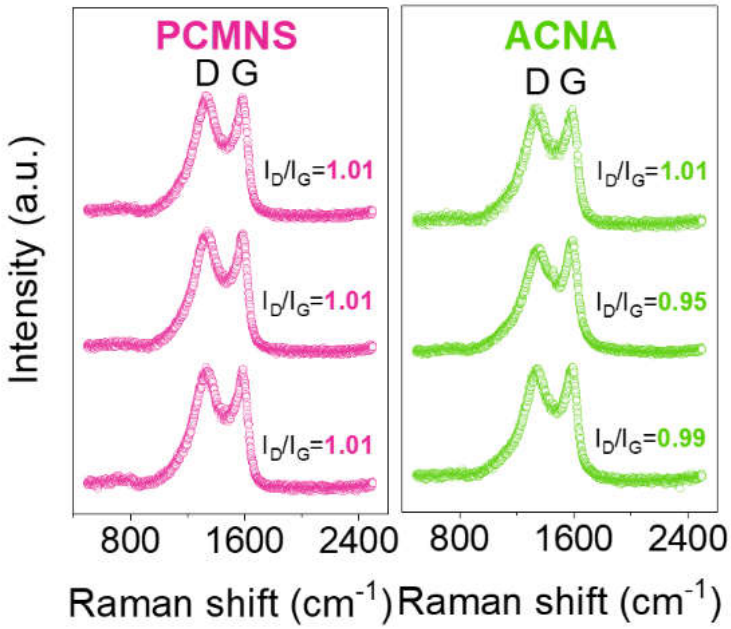

Figure S6. Raman spectra comparison between PCMNS and ACNA. Three Raman spectra were recorded randomly on three micro-domains within the identical sample. (PCMNS: Polyhedral Carbon Micro-Nano-Shells; ACNA: Amorphous Carbon Nano-Aggregates)

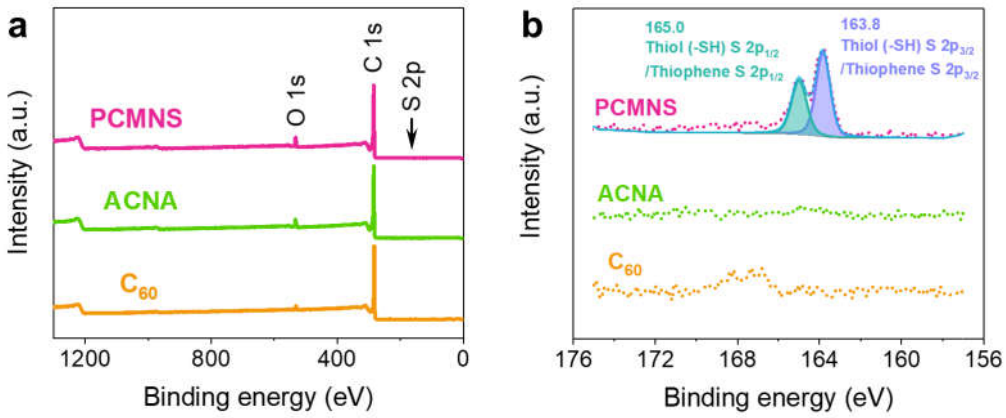

Figure S7. XPS comparison between PCMNS, ACNA and C_{60}: survey spectra (a) and detailed S 2p spectra (b). (PCMNS: Polyhedral Carbon Micro-Nano-Shells; ACNA: Amorphous Carbon Nano-Aggregates)

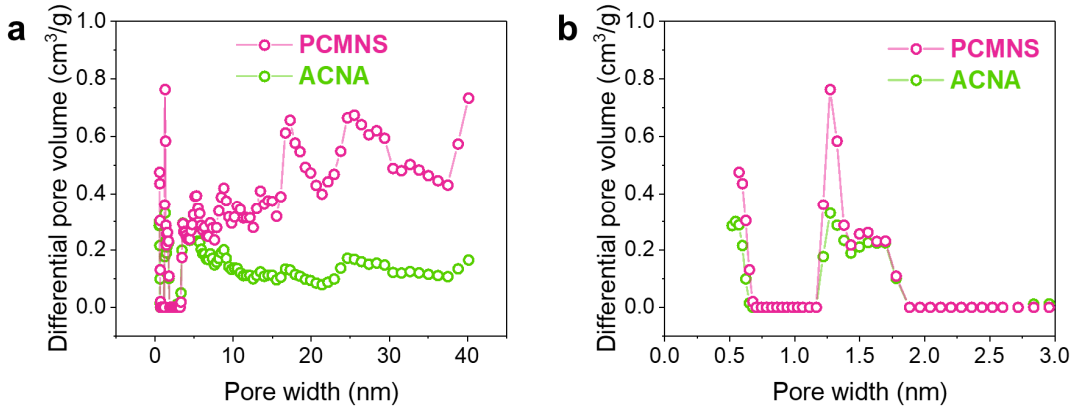

Figure S8. The pore volume-pore size distribution comparison between PCMNS and ACNA: pore width range of 0.5-40 nm (a) and 0.5-3.0 nm (b). (PCMNS: Polyhedral Carbon Micro-Nano-Shells; ACNA: Amorphous Carbon Nano-Aggregates)

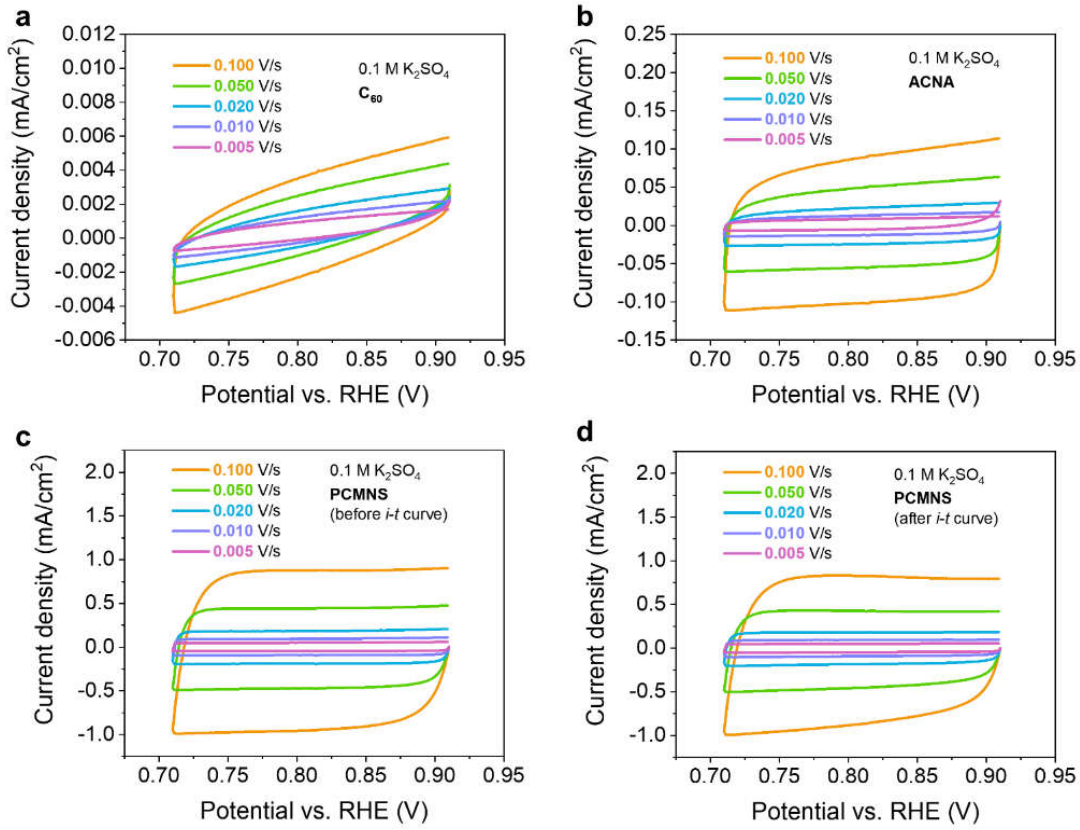

Figure S9. The electrochemical surface area (ECSA) of C_{60} (a), ACNA (b) and PCMNS (c & d) estimated by cyclic voltammetry curves on RRDE in 0.1 M K_2SO_4. (PCMNS: Polyhedral Carbon Micro-Nano-Shells; ACNA: Amorphous Carbon Nano-Aggregates)

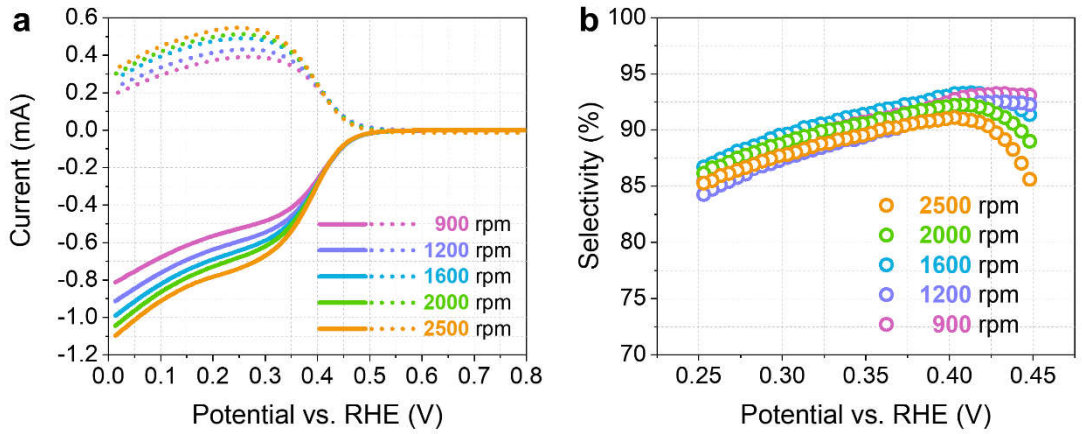

Figure S10. Linear sweep voltammetry curves (a) and selectivity-potential curves (b) of PCMNS recorded with different rotation speed. (PCMNS: Polyhedral Carbon Micro-Nano-Shells)

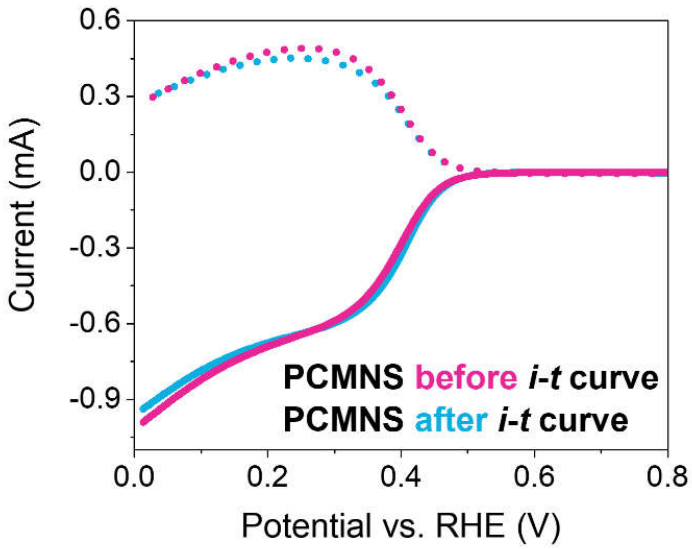

Figure S11. Linear sweep voltammetry curves of PCMNS recorded before and after stability test. (PCMNS: Polyhedral Carbon Micro-Nano-Shells)

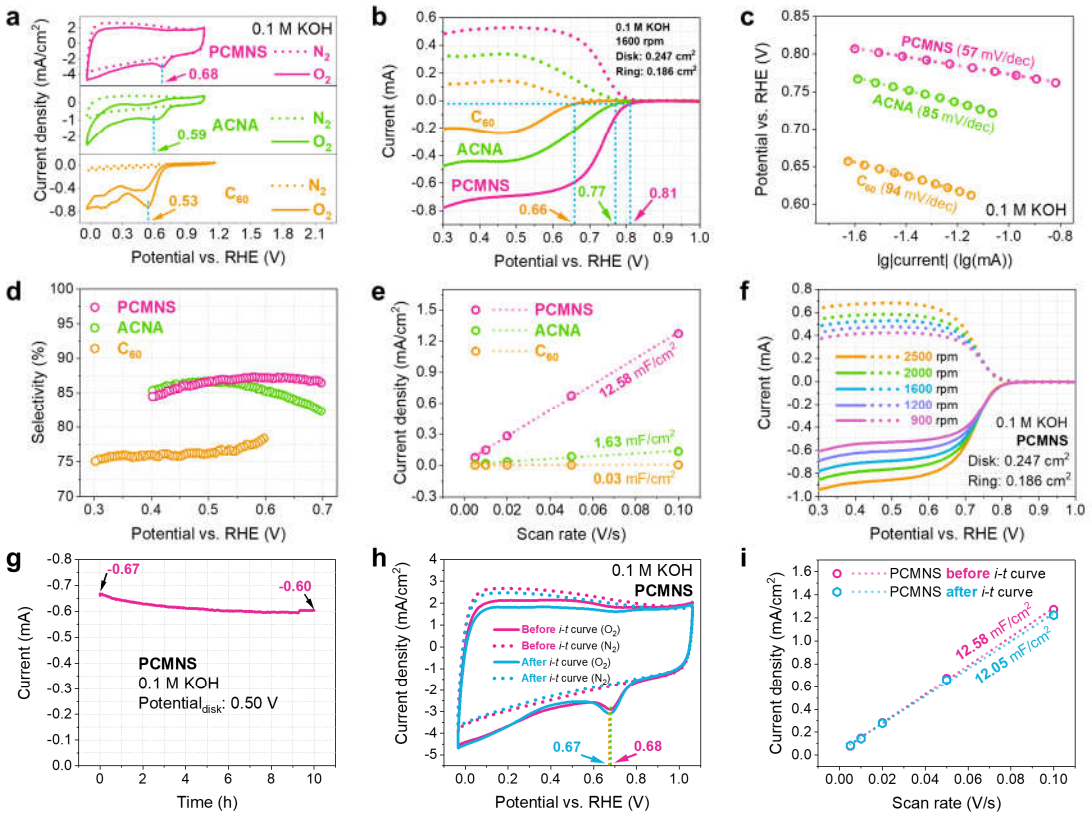

Figure S12. The electrocatalytic oxygen reduction reaction performance recorded on RRDE in 0.1 M KOH: cyclic voltammetry curves (a), linear sweep voltammetry curves (b), Tafel slopes (c), selectivity-potential curves (d) and electrochemical surface area (e) of PCMNS, ACNA and C_{60}. Linear sweep voltammetry curves of PCMNS recorded with different rotation speed (f). *i*-t curve of PCMNS (g), comparison of cyclic voltammetry curves (h) and electrochemical surface areas (i) before and after potentiostatic test of PCMNS. (PCMNS: Polyhedral Carbon Micro-Nano-Shells; ACNA: Amorphous Carbon Nano-Aggregates)

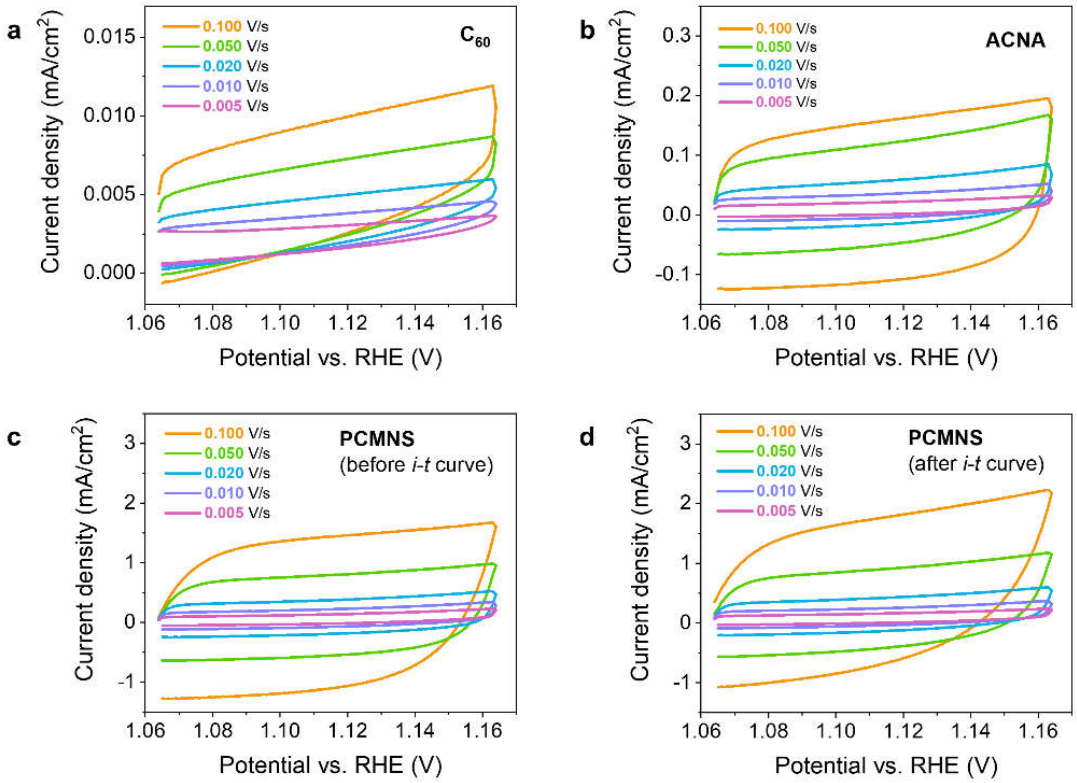

Figure S13. The electrochemical surface area (ECSA) of C_{60} (a), ACNA (b) and PCMNS (c & d) estimated by cyclic voltammetry curves on RRDE in 0.1 M KOH. (PCMNS: Polyhedral Carbon Micro-Nano-Shells; ACNA: Amorphous Carbon Nano-Aggregates)

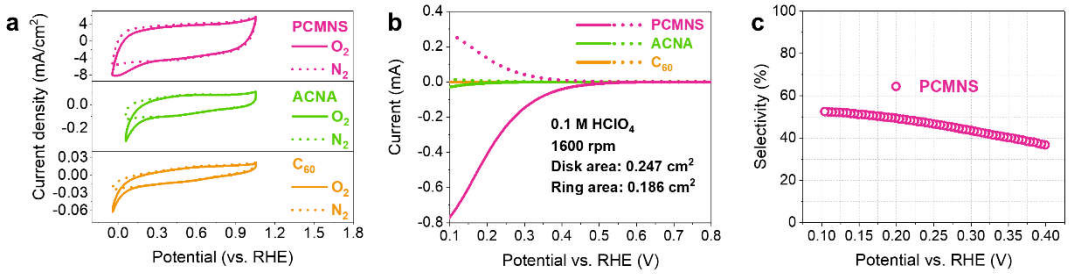

Figure S14. The electrocatalytic oxygen reduction reaction performance recorded on RRDE in 0.1 M $HClO_4$: cyclic voltammetry curves (a), linear sweep voltammetry curves (b), selectivity-potential curves (c) of PCMNS, ACNA and C_{60}. (PCMNS: Polyhedral Carbon Micro-Nano-Shells; ACNA: Amorphous Carbon Nano-Aggregates)

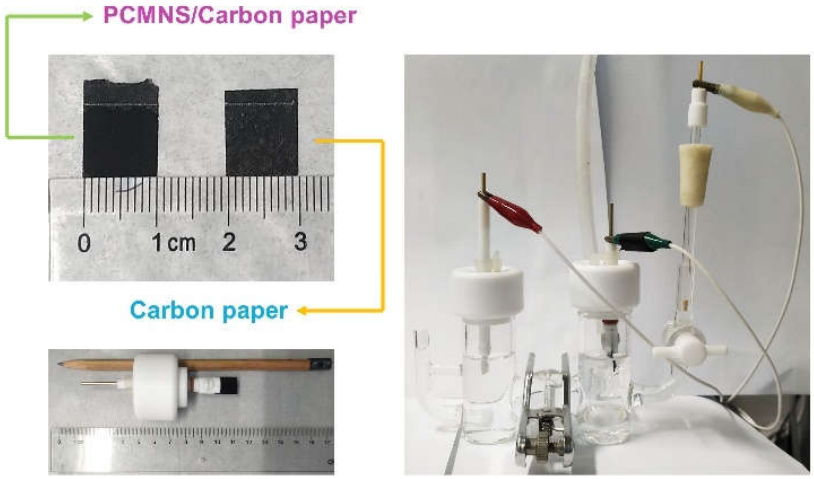

Figure S15. Practical photos of the PCMNS/Carbon paper electrode and the H-type electrolytic cell.

The direct relation between the absorbance value and the concentration of H_2O_2 was based on the following equations (eqs):

$$A=kC_{Ce^{4+}} \quad \text{(S1)}$$

$$=k(C_{i,Ce^{4+}}-2C_{H_2O_2}) \quad \text{(S2)}$$

$$=kC_{i,Ce^{4+}}-2kC_{H_2O_2} \quad \text{(S3)}$$

A means the absorbance value in Ultraviolet-visible-infrared absorption spectrum,

k means the proportional coefficient,

$C_{Ce^{4+}}$ means the concentration of residual Ce^{4+} in solution,

$C_{i,Ce^{4+}}$ means the initial concentration of the coloring solution,

$C_{H_2O_2}$ means the concentration of the synthesized H_2O_2.

Actually, the absorbance value is the proportional function of the concentration of residual Ce^{4+} in solution, as expressed in **eqs S1**. Based on the chemical reaction equation $2Ce^{4+}+H_2O_2 \rightarrow 2Ce^{3+}+O_2+2H^+$, the concentration of residual Ce^{4+} in solution is dependent on the concentration of the synthesized H_2O_2, as expressed in **eqs S2**. The consumed concentration of Ce^{4+} can be represented by the concentration of the synthesized H_2O_2, so it is natural to establish a direct relation between the absorbance

value and the concentration of the synthesized H_2O_2, as expressed in **eqs S3**.

The absorbance value-H_2O_2 concentration calibration curve was obtained by the following method:

1.0 mL coloring solution (5 mM Ce^{4+}) was mixed respectively with four 1.0 mL H_2O_2 solution of known concentration (labeled as TS1, TS2, TS3, TS4 in **Table.** The H_2O_2 solution of known concentration), then every mixture (the photos of all the reacted mixture are shown in **Figure S16a**) was diluted with 10.0 mL 0.1 M K_2SO_4 and shaken thoroughly. 3 of 12 mL liquid was transferred into cuvette for Ultraviolet-visible-near infrared absorption spectroscopy. The Ultraviolet-visible-near infrared absorption spectra are recorded as **Figure S16b**. Associating the highest absorbance value around 320 nm with the known H_2O_2 concentration, we fit the absorbance value-H_2O_2 concentration calibration curve as **Figure S16c**. Via the intercept and slope of the fitted curve, we can know the practical concentration of the coloring solution is 4.5 mM, which is very close to the theoretical value 5.0 mM. This concentration error is a comprehensive result of activity coefficient, experimental operation and measurement deviation.

Table. The H_2O_2 solution of known concentration

Label	9.77 M H_2O_2 (μL)	0.1 M K_2SO_4 (mL)	Concentration of H_2O_2 (mmol/L)
TS1	0	40	0
TS2	3	40	0.73
TS3	6	40	1.46
TS4	9	40	2.19

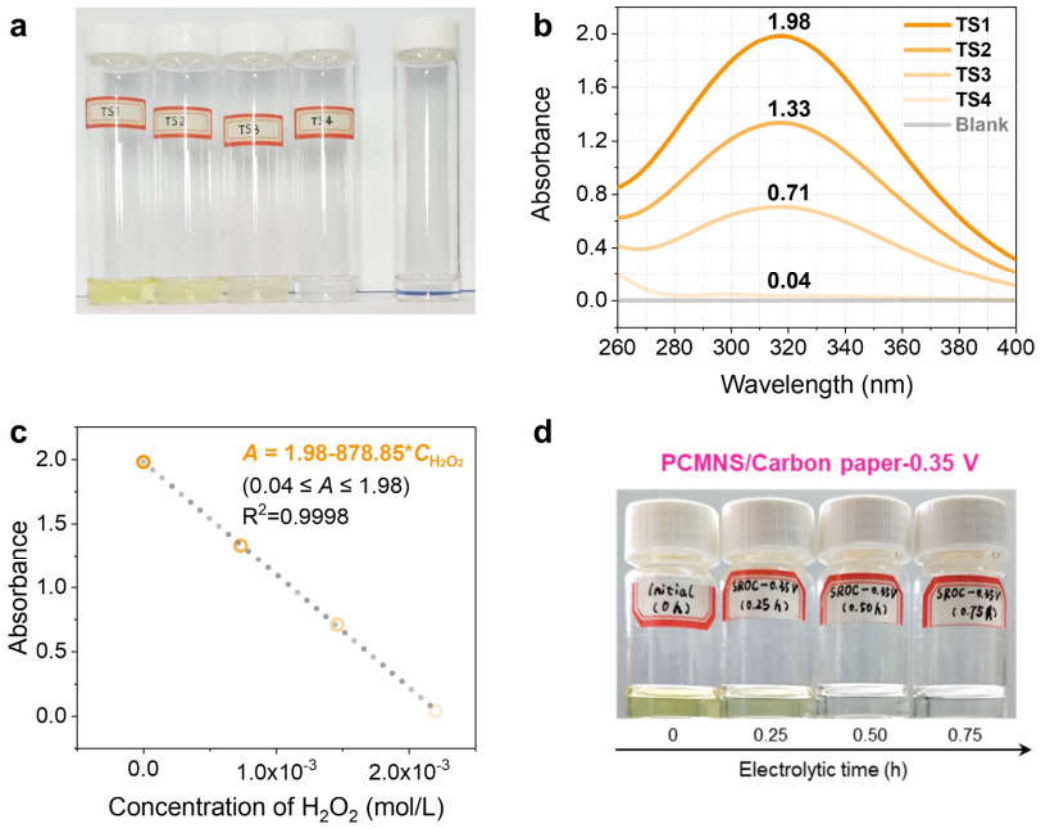

Figure S16. Practical photos (a) and Ultraviolet-visible-infrared absorption spectra (b) of the solution mixed by the same volume of coloring agent and different H_2O_2 solution of known concentration. Absorbance value-H_2O_2 concentration calibration curve (c). Practical photos of the solution mixed by the same volume of coloring agent and electrolyte extracted at different electrolytic time (d).

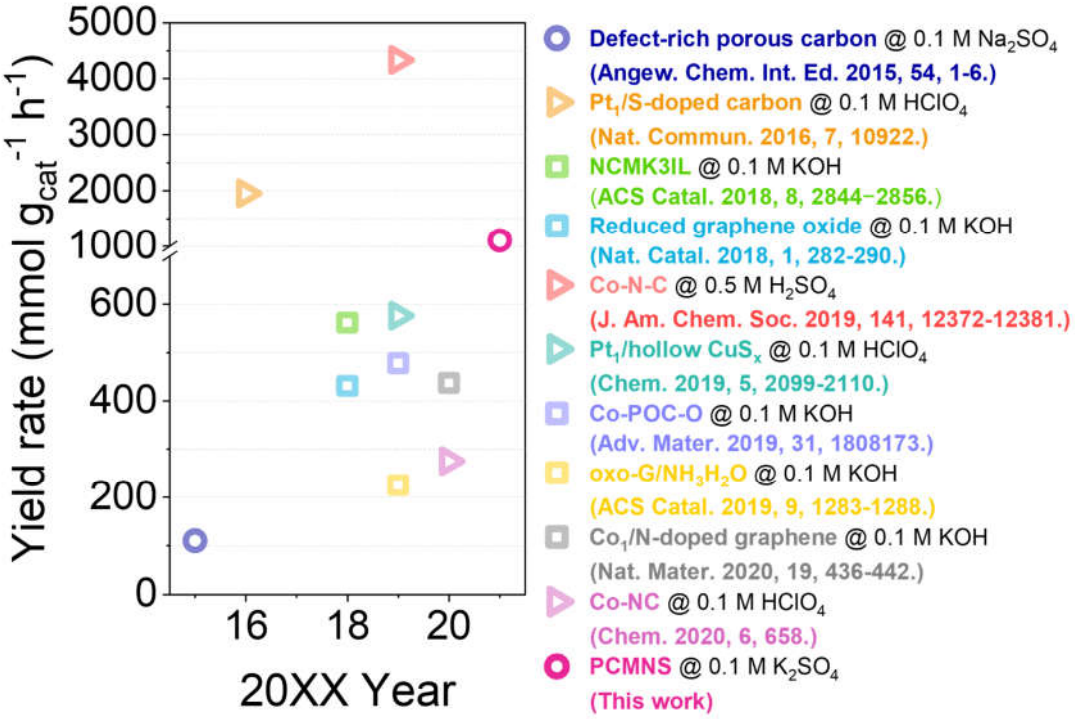

Figure S17. Yield rate comparison with the reported literatures.

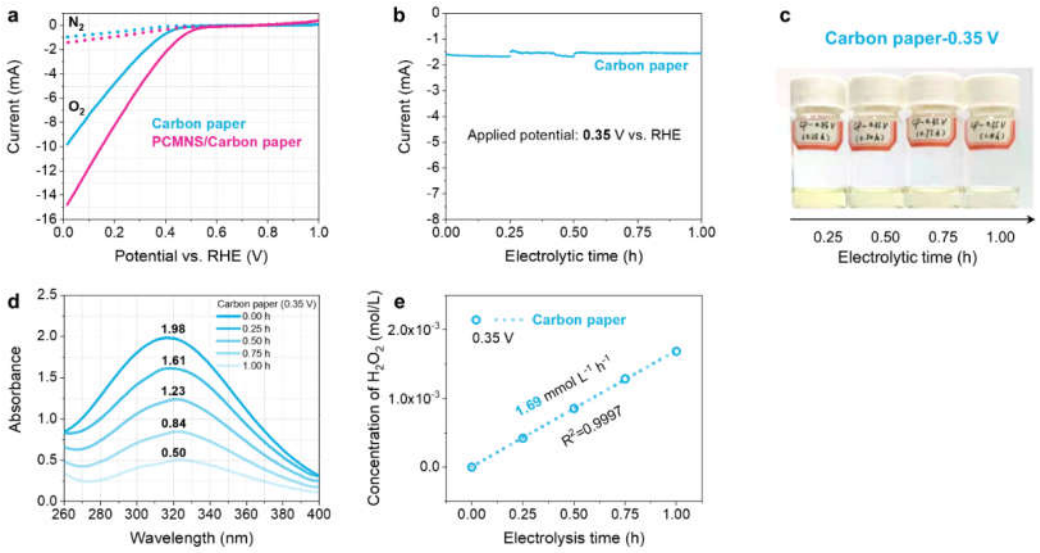

Figure S18. Linear sweep voltammetry curve (a) and *i-t* curve (b) of the Carbon paper electrode. Practical photos (c) and Ultraviolet-visible-near infrared absorption spectra (d) of the solution mixed by the same volume of coloring agent and electrolyte extracted at different electrolytic time. H_2O_2 concentration-electrolytic time curve (e).

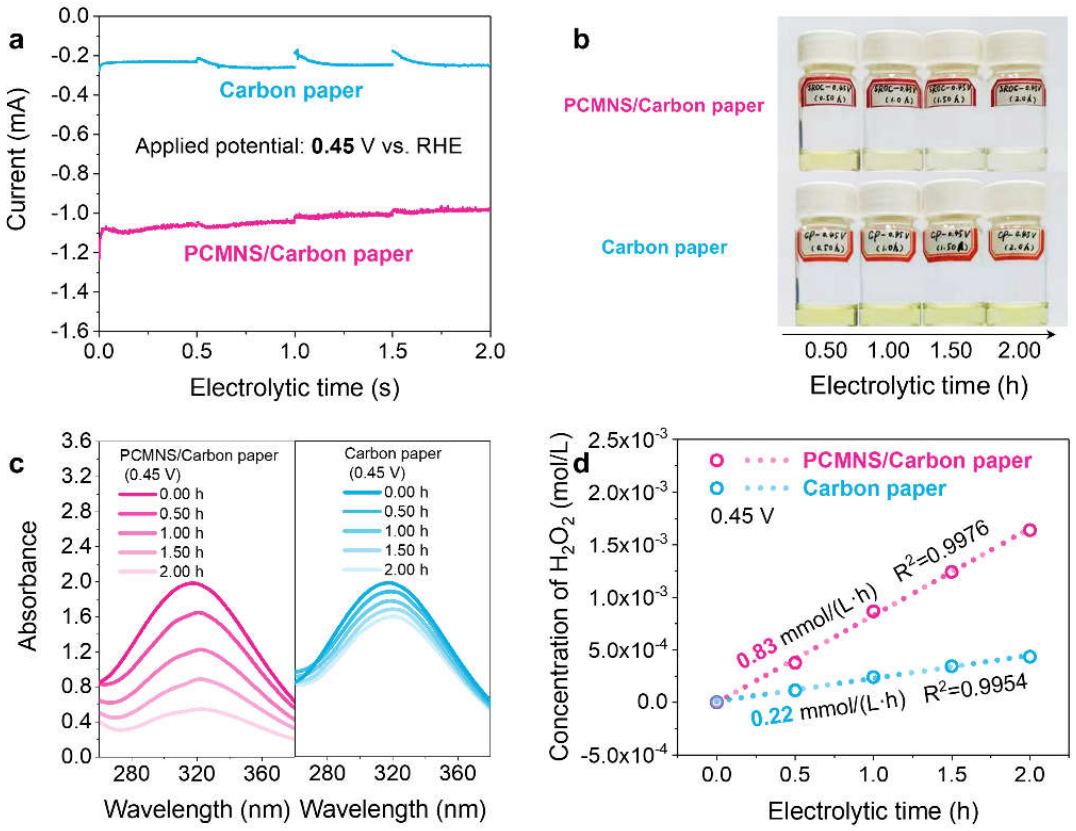

Figure S19. *I-t* curves with potential of 0.45 V (vs. RHE) of the Carbon paper electrode and PCMNS/Carbon paper electrode (a). Practical photos (b) and Ultraviolet-visible-near infrared absorption spectra (c) of the solution mixed by the same volume of coloring agent and electrolyte extracted at different electrolytic time. H_2O_2 concentration-electrolytic time curves (d).

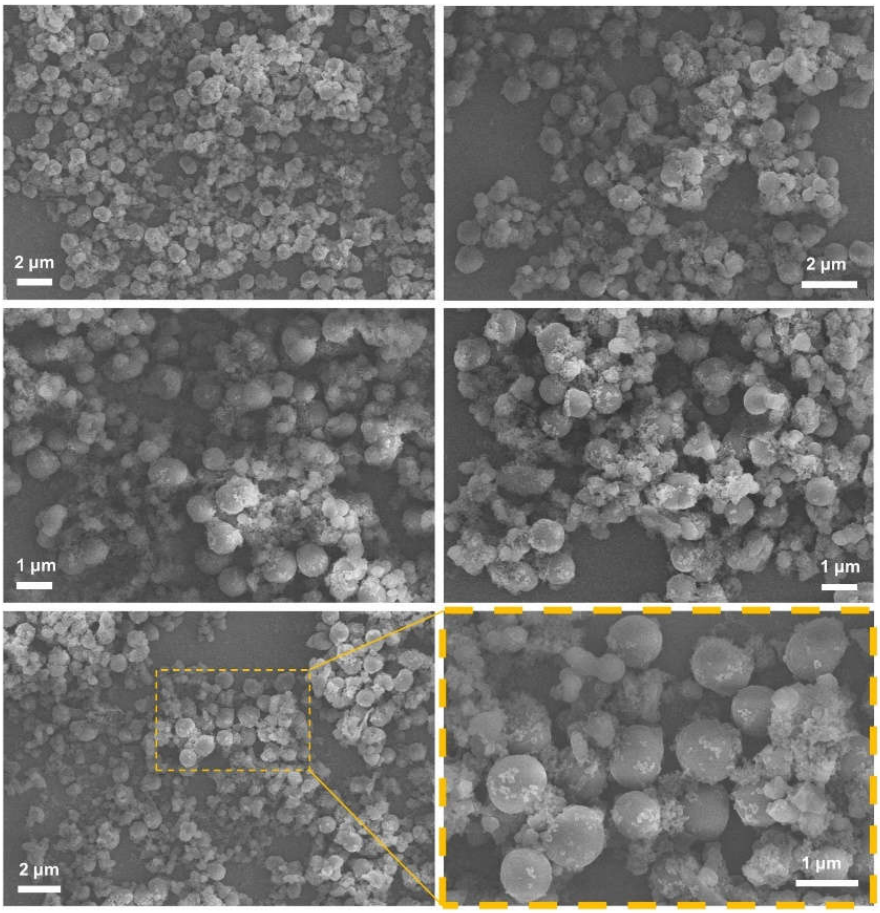

Figure S20. SEM images of "With thiophene".

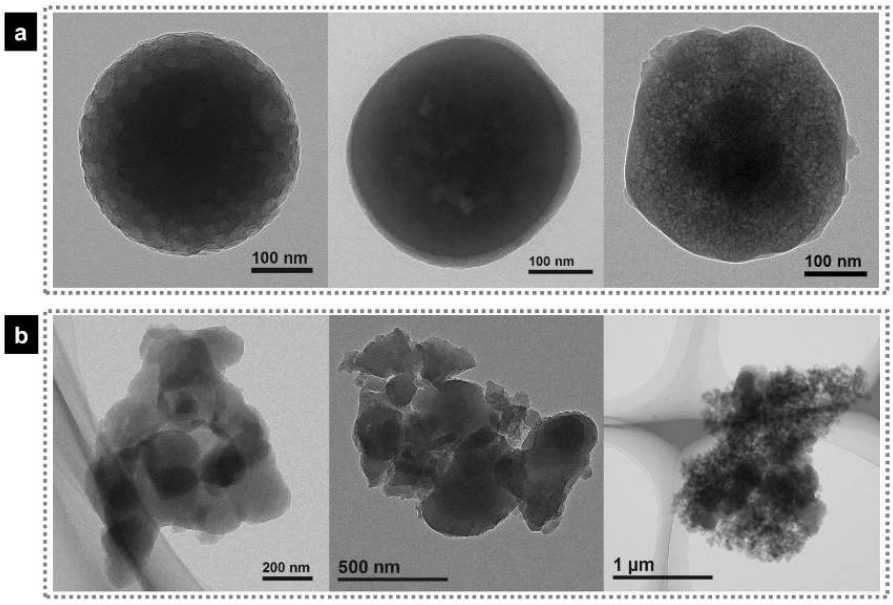

Figure S21. TEM comparison between "With thiophene" (a) and "Without thiophene" (b).

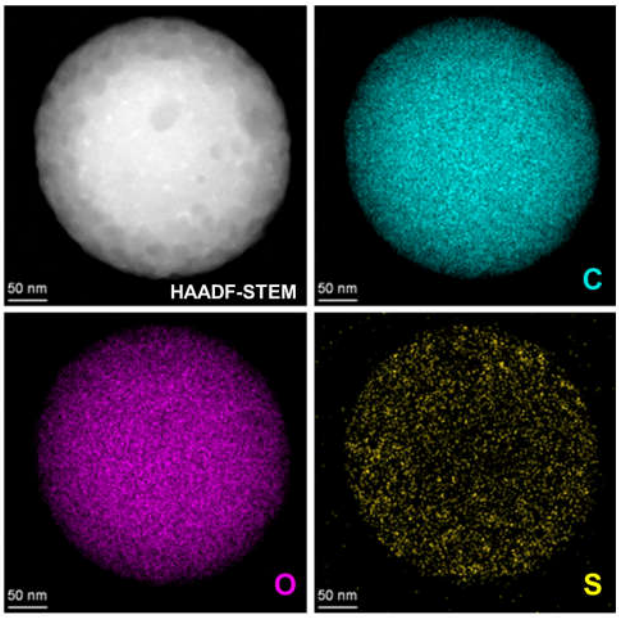

Figure S22. STEM images and EDS-elemental mapping of "With thiophene".

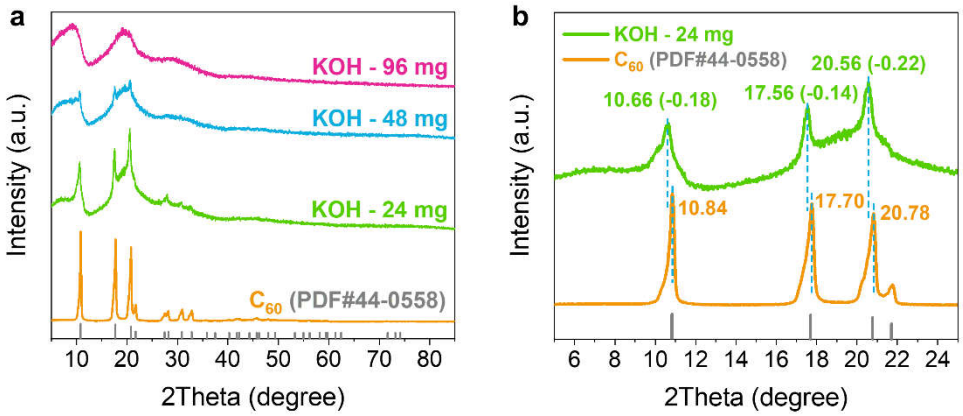

Figure S23. The impact of dosage of KOH on XRD patterns of "With thiophene" (a), the locally amplified XRD patterns of "With thiophene" (KOH-24 mg) and C_{60}.

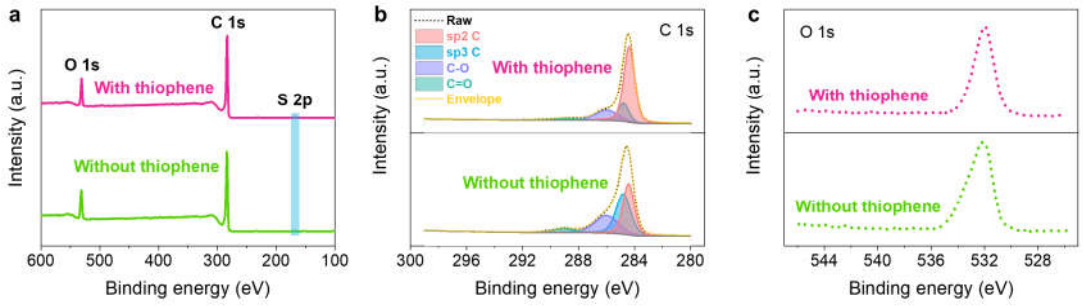

Figure S24. XPS comparison between "With thiophene" and "Without thiophene":

survey spectra (a), detailed C 1s spectra (b) and O 1s spectra (c).

Table S1. The element atomic percentage of PCMNS, ACNA and C_{60}.

(PCMNS: Polyhedral Carbon Micro-Nano-Shells; ACNA: Amorphous Carbon Nano-Aggregates)

Sample	Atomic percentage (%)		
	C	O	S
PCMNS	94.18	5.50	0.32
ACNA	95.23	4.77	0.00
C_{60}	97.05	2.95	0.00

Table S2. V-t method summary of PCMNS and ACNA.

(PCMNS: Polyhedral Carbon Micro-Nano-Shells; ACNA: Amorphous Carbon Nano-Aggregates)

V-t method summary		
	PCMNS	ACNA
Slope	17.263	13.491
Intercept	61.683	16.046
Correlation coefficient	0.999276	0.999386
Micropore area (m^2/g)	218.259	52.054
Mesopore area (m^2/g)	267.024	208.681
Specific surface area (m^2/g)	485.283	260.735

Table S3. The selectivity comparison with the other typical carbon-based nanomaterials.

(PCMNS: Polyhedral Carbon Micro-Nano-Shells)

Catalyst	Electrolyte	Selectivity (%)	Specific surface area (m2/g)	Reference
Defect-rich porous carbon	0.1 M Na_2SO_4	85	2130	*Angew. Chem. Int. Ed.* **2015**, 54, 1-6.
Reduced graphene oxide	0.1 M KOH	~100	None	*Nat. Catal.* **2018**, 1, 282-290.
N-doped carbon nanohorn	0.1 M PBS	90	271	*Chem* **2018**, 4, 1–18.
Oxidized carbon nanotube	0.1 M PBS	~88	None	*Nat. Catal.* **2018**, 1, 156–162.
Mo1/O,S-doped graphene	pH=8.7	77	None	*Angew. Chem. Int. Ed.* **2020**, 59, 9171– 9176.
Co1/N-doped graphene	0.1 M PBS	~70	None	*Nat. Mater.* **2020**, 19, 436-442.

PCMNS	**0.1 M K_2SO_4**	**86.7-93.3**	**485**	**This work**

Table S4. The reported yield rate of H_2O_2.

Catalyst	Electrolyte	Yield rate (mmol/g/h)	Reference
Defect-rich porous carbon	0.1 M Na_2SO_4	110	*Angew. Chem. Int. Ed.* **2015**, *54*, 1-6.
Pt_1/S-doped carbon	0.1 M $HClO_4$	~1950	*Nat. Commun.* **2016**, *7*, 10922.
NCMK3IL	0.1 M KOH	562	*ACS Catal.* **2018**, *8*, 2844-2856.
F-mrGO	0.1 M KOH	431	*Nat. Catal.* **2018**, *1*, 282-290.
Co-N-C	0.5 M H_2SO_4	~4330	*J. Am. Chem. Soc.* **2019**, *141*, 12372-12381.
Pt_1/hollow CuSx	0.1 M $HClO_4$	576	*Chem.* **2019**, *5*, 2099-2110.
Co-POC-O	0.1 M KOH	478	*Adv. Mater.* **2019**, *31*, 1808173.
oxo-G/NH_3H_2O	0.1 M KOH	225	*ACS Catal.* **2019**, *9*, 1283-1288.
Co_1/N-doped graphene	0.1 M KOH	437	*Nat. Mater.* **2020**, *19*, 436-442.
Co-NC	0.1 M $HClO_4$	275	*Chem.* **2020**, *6*, 658.
O-CNTs	0.1 M KOH	-	*Nat. Catal.* **2018**, *1*, 156-162.
Fe-CNT	0.1 M PBS	-	*Nat. Commun.* **2019**, *10*, 3997.
PCMNS	0.1 M K_2SO_4	1103	This work

Table S5 Element contents of "With thiophene" and "Without thiophene" from Element Analysis.

Sample	Percentage of weight (w.t.%)				
	C	O	S	H	N
With thiophene	79.94	15.42	3.04	1.30	≤0.30
	79.62	15.44	3.12	1.52	≤0.30
Without thiophene	90.27	7.59	0.46	1.38	≤0.30
	90.05	7.88	0.71	1.06	≤0.30